Efficient Spin Interconversion by Molecular Conformation Dynamics of a Triplet Pair for Photon Up-Conversion in an Amorphous Solid

Okamoto, Tsubasa
Izawa, Seiichiro
Hiramoto, Masahiro
Kobori, Yasuhiro

(Citation)
The Journal of Physical Chemistry Letters,15(11):2966-2975

(Issue Date)
2024-03-21

(Resource Type)
journal article

(Version)
Version of Record

(URL)
https://hdl.handle.net/20.500.14094/0100487697

THE JOURNAL OF PHYSICAL CHEMISTRY LETTERS
A JOURNAL OF THE AMERICAN CHEMICAL SOCIETY

pubs.acs.org/JPCL
Letter

Efficient Spin Interconversion by Molecular Conformation Dynamics of a Triplet Pair for Photon Up-Conversion in an Amorphous Solid

Tsubasa Okamoto,* Seiichiro Izawa,* Masahiro Hiramoto, and Yasuhiro Kobori*

Cite This: J. Phys. Chem. Lett. 2024, 15, 2966−2975
Read Online

ACCESS | Metrics & More | Article Recommendations | Supporting Information

ABSTRACT: Solid-state materials with improved light-to-energy conversions in organic photovoltaics and in optoelectronics are expected to be developed by realizing efficient triplet−triplet annihilation (TTA) by manipulating the spin conversion processes to the singlet state. In this study, we elucidate the spin conversion mechanism for delayed fluorescence by TTA from a microscopic view of the molecular conformations. We examine the time evolution of the electron spin polarization of the triplet-pair state (TT state) in an amorphous solid-state system exhibiting highly efficient up-conversion emission by using time-resolved electron paramagnetic resonance. We clarified that the spin-state population of the singlet TT increased through the spin interconversion from triplet and quintet TT states during exciton diffusion with random orientation dynamics between the two triplets for the modulation of the exchange interaction, achieving a high quantum yield of up-conversion emission. This understanding provides us with a guide for the development of efficient light-to-energy conversion devices utilizing TTA.

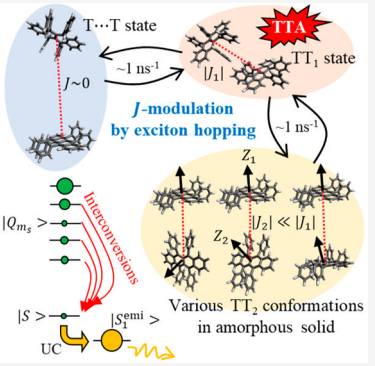

Triplet−triplet annihilation (TTA) is a fundamental process in which two triplets encounter and interact with each other.[1] Many research groups have worked on fundamental studies of the TTA process since the middle of the 20th century.[2] In particular, it is well known that the TTA process goes through a transition state in which two triplets are coupled via an exchange interaction following triplet-pair (TT) formation[1,3−7] as well as the activation for ultimate triplet separations from the exchange-coupled TT in the singlet fission (SF) which is the reverse process of TTA.[8] The electronic and magnetic interactions between two triplets depend on the local molecular orientation created by the geometry of the TT states.[9,10] However, the TTA mechanism has not been fully elucidated in this viewpoint, although an understanding of those interactions is of great importance to research areas such as quantum entanglement,[11−13] physics related to entangled bosons, and quantum information science.[14−16] Furthermore, the development of novel energy-conversion technologies utilizing the TTA process has also been widely explored with the aim of solving social issues. For example, the up-conversion (UC) technique through the TTA process (TTA-UC) has attracted researchers in several fields related to light-to-energy conversion technologies. In this regard, it is expected that the TTA-UC system contributes not only to commercializing highly efficient OLED devices,[17−22] solar cells,[23−28] and photocatalysts[29] but also to bringing about innovation in biomedical fields[30−33] such as photodynamic therapy,[34] drug delivery systems,[35] optogenetics,[36] and bioimaging.[37]

The TTA-UC system is basically composed of sensitizer and emitter molecules and is realized through several elementary processes. The quantum yield of UC emission (Φ_{UC}), that is, the fraction of the number of emitted photons to the number of absorbed photons, depends on the quantum efficiency of each elementary process. Φ_{UC} is described as follows

$$\Phi_{UC} = \frac{1}{2}\Phi_{Abs}\Phi_{ISC}\Phi_{TET}\Phi_{TTA}\eta\Phi_{Flu} \quad (1)$$

where Φ_{Abs}, Φ_{ISC}, Φ_{TET}, Φ_{TTA}, and Φ_{Flu} are the quantum yields of photon absorption by the sensitizer, intersystem crossing in the sensitizer, triplet−triplet energy transfer from the sensitizer to the emitter, TTA between two emitters, and the fluorescence of the emitter, respectively. The coefficient 1/2 indicates that the maximum value of Φ_{UC} is 50% because TTA-UC is a process in which two lower-energy photons are converted to one higher-energy photon. Also, η, which is often called the spin-statistical factor, is the probability of yielding a first-excited emissive singlet (S_1^{emi}) from all of the possible spin multiplicities of singlet, triplet, and quintet TT character. A small η of 11% is anticipated according to the spin statistics by the triplet−triplet encounter. A short triplet lifetime of the emitter molecule can be another possible factor reducing Φ_{UC}.[38] To achieve Φ_{UC} close to the upper limit of 50%, it is required that each process in eq 1 proceeds efficiently within

Received: December 26, 2023
Revised: February 10, 2024
Accepted: February 20, 2024
Published: March 13, 2024

the triplet-state lifetime. For example, a TTA-UC system composed of platinum-octaethylporphyrin (PtOEP) and 9,10-diphenylanthracene (DPA) is one of the most famous TTA-UC systems and exhibits the highest Φ_{UC} value among all reported TTA-UC samples.[39] In this system, Φ_{Abs}, Φ_{ISC}, Φ_{TET}, Φ_{TTA}, and Φ_{Flu} are as high as 90−100%. However, the Φ_{UC} is about 20% due to a low η of about 40%.[39] Also in this case, a low η is a bottleneck in the respective TTA-UC systems, but mechanisms of determining η and related strategies to improve the UC have not been presented.[40] To resolve these problems, it is necessary to investigate the molecular conformation effects of the spin-state characteristics during the TTA process. Several studies have discussed the spin state of the TT in the TTA process in both solid and liquid phases. Magneto-luminescence (ML) effects on the TTA processes were studied in the 1960s and 1970s.[1,3,5,6,41] In these, the theoretical reaction models considering the TT state were proposed. In recent research on TTA-UC, the spin state of the TT has often been discussed based on a simple model in which two triplets are coupled with strong exchange interaction causing one singlet-TT sublevel ($|S\rangle$), three triplet-TT sublevels ($|T_{m_{s,T}}\rangle$) and five quintet-TT sublevels ($|Q_{m_{s,Q}}\rangle$),[41−44] where m_s represents the spin angular momentum ($m_{s,Q} = \pm 2, \pm 1, 0$ for the quintet and $m_{s,T} = \pm 1, 0$ for the triplet), respectively. In the TTA process, populations of all nine spin sublevels of the TT are equally 11.1% according to the spin statistics in the initial encounter. Only η = 11.1% in TTs can thus contribute to the TTA-UC from the spin-statistical limit.[45] However, for an actual TTA-UC system such as PtOEP/DPA, η is beyond this limit.[40,46−51] The TTA reaction models used to explain the experimental results were proposed in a few reports.[10,52,53] They have investigated the ML effects in the TTA-UC system and proposed the UC pathways with which three different molecular conformations are involved in the TT states in the crystalline systems. Also, spin dynamics of the TTA process is important because the TTA process requires spatial motions of excitons during the encounter with the counterpart exciton. Several groups have discussed such spin dynamics of TT in investigations of the ML effects of the liquid TTA-UC systems.[54−56] However, the mechanism exceeding η = 11.1% is not clear in the disordered environments such as in amorphous solid. In particular, spin-state populations in the TT state, i.e., populations of the nine diabatic spin characters of the singlet, triplet, and quintet TTs, have not been investigated in the TTA-UC system.[10] The observation of the time dependence of electron spin polarization (ESP) caused by the spin-state populations is often fruitful in understanding the local electronic structure of the transient TT such as a distance and a mutual orientation between two triplets.[13] By investigating the time evolution of ESP during the TTA process, one can expect to elucidate its mechanism by taking into consideration the exciton mobility and conformation.[9] Concerning the TTA-UC, liquid-phase TTA-UC systems were extensively examined.[42] However, the quick random rotation of the emitter molecule prevents us from observing the magnetic anisotropy by the spin dipolar coupling of the triplet in the solutions, and thus, they are not suitable for studying the effect of the conformation on the ESP. A solid-state TTA-UC system can be useful for studying the spin state from the microscopic viewpoints when the exciton diffusion is not significantly high.

To reveal the TTA-UC mechanism exhibiting high η and Φ_{UC} in the disordered system, we performed continuous-wave time-resolved electron paramagnetic resonance (TREPR) measurements of a solid-state film as a TTA-UC sample to characterize the ESP of the triplet state in the emitter. Figure 1a shows a schematic cross-sectional view of the film sample

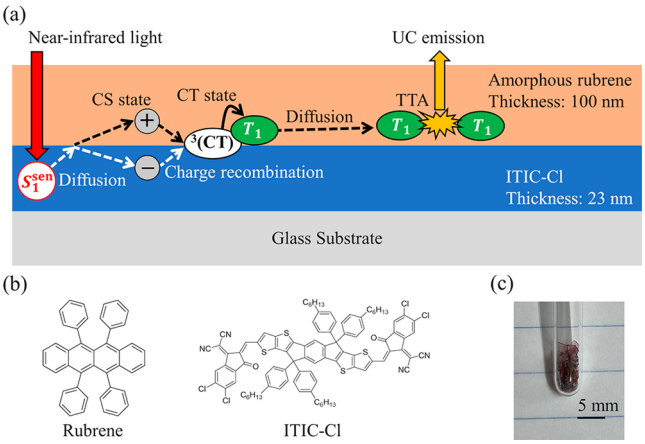

Figure 1. (a) Cross-sectional view of the rubrene/ITIC-Cl bilayer sample used in this study. Flow of the TTA-UC process through a former process in which the triplet exciton is generated at the rubrene/ITIC-Cl interface is schematically shown. As a substrate, we used a cover glass (C018181, Matsunami Glass Ind., Ltd.) in which the area was 1.8 × 1.8 mm^2 and the thickness was on the order of 0.1 mm. (b) Molecular structures of rubrene (left) and ITIC-Cl (right). (c) Picture of the sample in the EPR quartz tube.

used in this study. This sample is composed of two layers—an amorphous rubrene layer as the emitter (or donor) and a 3,9-bis(2-methylene-((3-(1,1-dicyanomethylene)-6,7-dichloro)-indanone))-5,5,11,11-tetrakis(4-hexylphenyl)-dithieno[2,3-d:2′,3′-d′]-s-indaceno[1,2-b:5,6-b′]dithiophene (ITIC-Cl) layer as the sensitizer (or acceptor)—and exhibits a high η value of 64%.[57,58] It is reported that the upconversion efficiency of the bulk heterojunction (BHJ) film of rubrene/ITIC-Cl was significantly lower than that of the planar heterojunction (PHJ).[59] Therefore, the PHJ film is more suitable for the up-conversion application. In addition, a multilayer amorphous film of rubrene/ITIC-Cl cannot be prepared because the underlying rubrene layer will be dissolved and crystallized when the ITIC-Cl is spin-coated repeatedly. For these reasons, we prepared a bilayer film in this study. Rubrene (Tokyo chemical industry, sublimed grade) and ITIC-Cl (Ossila) were used without further purification. ITIC-Cl (right-hand side of Figure 1b) was spin-coated on the glass substrate. After that, rubrene (left-hand side of Figure 1b) was deposited on top of the ITIC-Cl layer by thermal deposition under high-vacuum conditions (~10^{-5} Pa). The film thicknesses of the layers were measured by using a surface profilometer (Dektak 150, Veeco). The thicknesses of the rubrene and ITIC-Cl layers were 100 and 23 nm, respectively. Because the sample film was too large to be loaded into an EPR quartz tube (outer diameter 5 mm, inner diameter 4 mm), it was manually cut into several pieces and loaded into the EPR tube, as shown in Figure 1c. This ensures enough optical density for the 720 nm laser absorption because the irradiation path length is long enough due to the overlapping multiple cut films. Finally, the sample space was purged with nitrogen gas to prevent deterioration. In this sample, the TTA-

https://doi.org/10.1021/acs.jpclett.3c03602
J. Phys. Chem. Lett. 2024, 15, 2966−2975

UC process can be induced by the irradiation of infrared light as shown in Figure 1a. Incident infrared light is absorbed by the ITIC-Cl layer, and the first-excited singlet (S_1^{sen}) is generated and diffuses in the layer. Previous reports showed that the translational diffusion lengths of the S_1^{sen} in the ITIC series or nonfullerene acceptors are on the order of 10 nm.[60−63] Therefore, we consider that most of the excitons in ITIC-Cl reach the interface of rubrene and ITIC-Cl layers. At the interface, charge-separated states are created at the rubrene/ITIC-Cl interface. These separated free charges are encountered at the interface. Because the energy of the re-encountered triplet charge-transfer (CT) state is higher than the energy of the locally excited triplet rubrene molecule, the first excited triplet (T_1) is formed by the bimolecular recombination in the rubrene layer. Subsequently, T_1 diffuses in the rubrene layer for the TTA-UC.

The TREPR measurements were performed using a Bruker EMXplus spectrometer at 80 K. It is noted that we obtained the temperature dependence of the TTA-UC emission intensity in this system as shown in Figure S1. This confirms that TTA-UC occurs even at 80 K. Light excitation was performed by combining the third harmonic (355 nm) of a Nd:YAG laser with an optical parametric oscillator (Continuum Surelite OPO Plus, fwhm = 5 ns). The wavelength of the excitation light was 720 nm. A light depolarizer was placed between the laser output and the optical window of the EPR cavity. The excitation light power was 5.5 mJ/pulse, which corresponds to an excitation light power density (I_{ex}) of 194 mW/cm^2. Because the TTA process is one of the bimolecular reaction processes, the probability of the TTA event depends on the I_{ex} value.[38,64] It has been investigated that the threshold intensity (I_{th}), which is the lower limit at which TTA becomes the dominant quenching process of the triplet state, is 39 mW/cm^2 for the rubrene/ITIC-Cl system at room temperature.[57] The I_{th} value of the rubrene/ITIC-Cl system at low temperature has not been investigated and may be higher than that at room temperature. We checked the dependence of the I_{ex} on the intensity of the spin-polarized EPR signal obtained at two magnetic fields (345 and 360 mT) as shown in Figure S2. The slope of the double logarithmic plot at 360 mT exceeds 2 in the low power range. On the other hand, this slope is smaller than 2 and reaches 1 in a higher power range. This demonstrates that the EPR signals are generated by a combination of the following two bimolecular reaction processes: 1) the electron−hole recombination by the interfacial free carriers to the triplet product and 2) the subsequent TTA. More details are described in Figure S2.

Figure 2 shows the TREPR spectra of the rubrene/ITIC-Cl bilayer film obtained at 80 K. The delay time after the irradiation of excitation light is shown on the right side of each TREPR spectrum in this figure. The signals above and below the baseline correspond to microwave absorption (A) and emission (E), respectively. Intense emission signals are mainly observed in the magnetic field range from 320 to 370 mT, suggesting that this broad component originates from spin−spin dipolar interaction in the triplet exciton of the rubrene molecule for the TTA-UC process. In addition, weak, sharp emission signals are also observed in the center field for g = 2.00 (340 mT). The emissive signal reached a maximum intensity at about 0.6 μs. Time evolutions of the EPR signal intensities at 345 and 360 mT are shown in Figure S3.

To interpret the asymmetric line shapes of the TREPR spectra in Figure 2 with the emissive polarization in the

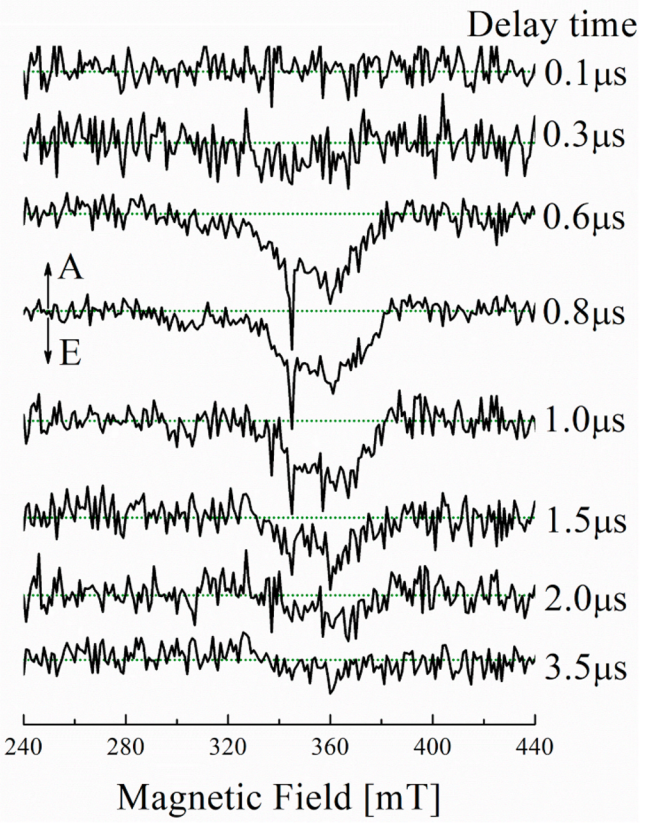

Figure 2. TREPR spectra of the rubrene/ITIC-Cl bilayer film obtained at several delay times after the excitation light was used to irradiate. The green dotted line is the baseline for each delay time. The microwave power and frequency were 20 mW and 9.672 GHz, respectively.

exciton, we consider the development of the TT states created by the encounter of the separated triplet excitons, as shown in Scheme 1. At first, one triplet exciton diffuses in the rubrene layer and encounters another triplet via the bimolecular process, resulting in the formation of TT. The distance between two triplets becomes very small and strongly coupled via the exchange interaction (J). The energy differences between $|S\rangle$ and $|T_{m_{s,T}}\rangle$ and between $|T_{m_{s,T}}\rangle$ and $|Q_{m_{s,Q}}\rangle$ are represented by $2J$ and $4J$, respectively. Under the strongly exchange-coupled state ($J = J_1$ in Scheme 1), because the energy levels in $|S\rangle$, $|T_{m_{s,T}}\rangle$, and $|Q_{m_{s,Q}}\rangle$ are highly separated, only the singlet TT can be converted to the first excited singlet $|S_1^{semi}\rangle$ by TTA. Remaining TTs can undergo T-T dissociation by the exciton diffusion in the rubrene domain. When the exchange interaction becomes weak ($|J| = |J_2| < |J_1|$ in Scheme 1), the energy differences between $|S\rangle$ and $|Q_{m_{s,Q}\le 0}\rangle$ become small enough to allow the spin conversion between $|S\rangle$ and $|Q_{m_{s,Q}\le 0}\rangle$ by the level crossing mechanism in the presence of the external magnetic field.[65] The conversion is also possible between $|T_{m_{s,T}}\rangle$ ($m_{s,T}$ = 1, 0, −1) and $|Q_{m_{s,Q}}\rangle$ ($m_{s,Q}$ = 1, 0, −1) with $m_{s,T} = m_{s,Q}$ in highly separated TT with $|J| = 0$. Due to random exciton diffusion in the rubrene film, the strength of exchange coupling becomes strong and weak repeatedly. Thanks to such a modulation of J, the $|T_{m_{s,T}}\rangle$ and $|Q_{m_{s,Q}}\rangle$ diabatic characters can be consumed by the TTA via the spin conversions, realizing the efficient TTA-UC.[57] On the other

https://doi.org/10.1021/acs.jpclett.3c03602
J. Phys. Chem. Lett. 2024, 15, 2966−2975

Scheme 1. Model of the TTA-UC Process in the Amorphous Rubrene Film for the Emissive TREPR[a]

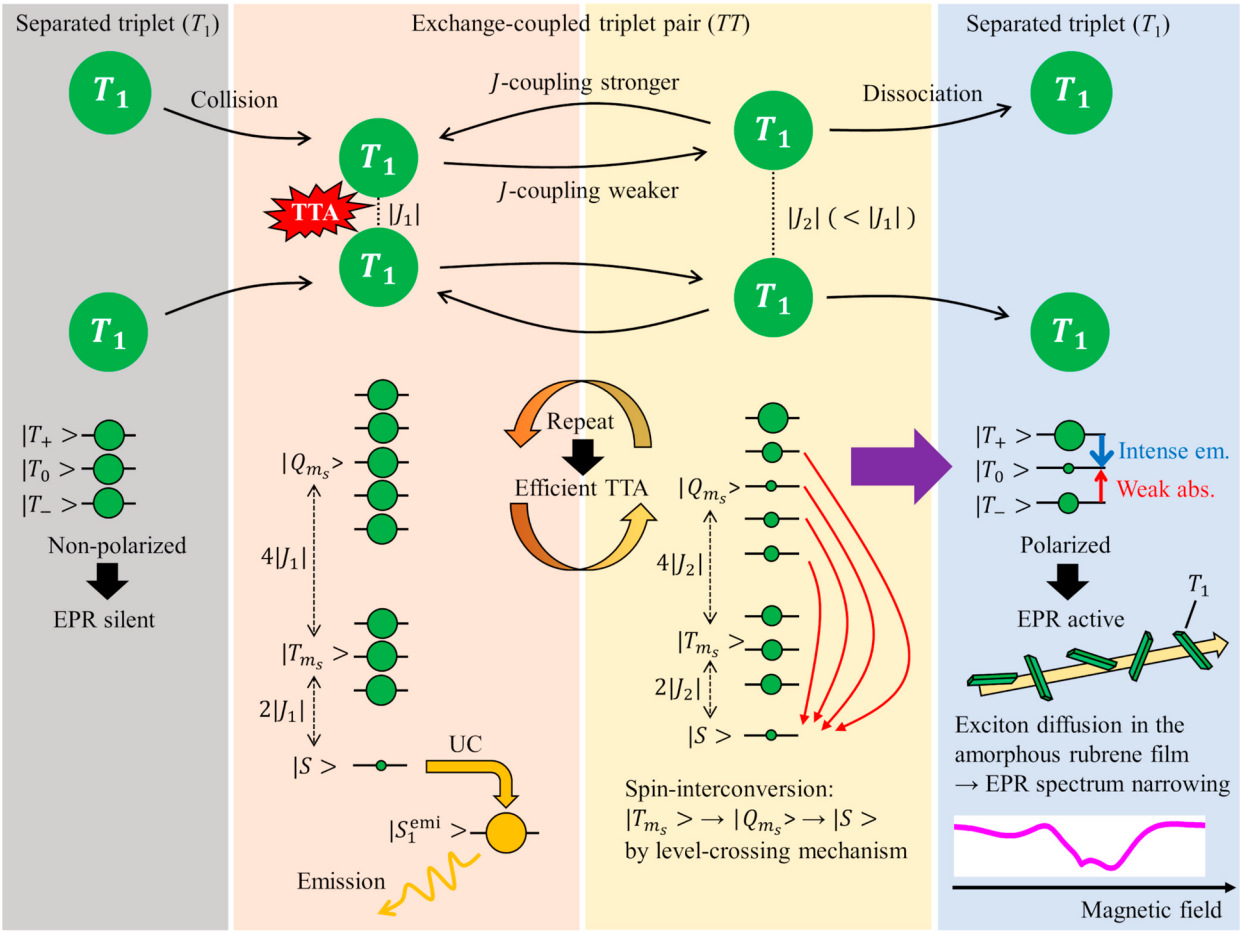

[a]The left gray part shows separated triplet states before TTA. The center red and yellow parts show encountered coupled TTs. The right blue part shows the separated triplet state after the TTA. Bottom parts show spin states of individual triplets and TTs. Sublevel populations are developed during TTA and dissociation. The bottom right shows the expected EPR spectrum when T_+ is overpopulated in the separated triplet and the exciton rotates during the exciton diffusion in the amorphous phase.

hand, the residual triplets can be completely isolated (right blue part of Scheme 1) after TTA in the presence of the external magnetic field. Here, the amounts of transferred spin from each sublevel of $|T_{m_{s,T}}\rangle$ and $|Q_{m_{s,Q}}\rangle$ to $|S\rangle$ are determined by the interactions represented by $\langle T_{m_{s,T}}|\mathbf{H}_{ZFS}|S\rangle$ and $\langle Q_{m_{s,Q}}|\mathbf{H}_{ZFS}|S\rangle$, respectively, where $\mathbf{H}_{ZFS}$ represent the zero-field splitting (ZFS) interaction by the dipolar coupling within the triplet exciton.[9] When negative J coupling is applied, the $|Q_{+2}\rangle$ sublevel is isolated from these spin conversions because this level does not undergo the level crossing in the high-field limit. This $|\alpha\alpha\alpha\alpha\rangle$ thus generates the TTA-induced ESP in the TT state with an emissive spin polarization. In contrast, isolated triplet states (T_+, T_0, and T_-) generated after the SF are reported to possess the dominant sublevel population in $|T_0\rangle$, while the lowest sublevel $|T_-\rangle$ had more population than that in the upper sublevel $|T_+\rangle$.[65,66] "AEE-AAE" (A, absorption; E, emission) pattern line shapes of triplet TREPR spectra were reported in the SF system in the TIPS-pentacene and TIPS-tetracene thin films[13,67] and in the pentacene dimer.[8] Because the TTA is an inverse process of SF, we expect that the separated triplet state after the TTA exhibits an inverse pattern of the ESP compared with the pattern in the SF system, as shown in the right blue part of Scheme 1. This ESP pattern corresponds to the "EAA-EEA" pattern line shape of the EPR spectrum, as shown at the top of Figure S4, although the TREPR spectrum does not exhibit clear fine structure, as shown in Figure 2. In amorphous rubrene, the orientation between adjacent rubrene molecules is random. Thus, the triplet exciton diffuses by randomly rotating its principal axes of the spin−spin dipolar coupling about the direction of the external magnetic field. When the exciton rapidly rotates, it is expected that the line width of the EPR spectrum becomes small due to the motional narrowing effect.[68] To prove the above hypothesis about the spin characters and the mobility of the triplet exciton, we performed line shape analysis using a spectrum simulation for an isolated triplet state. For this, we first determined sublevel populations (Figure 3) in the isolated triplet excitons on the diffusing excitons. Next, we simulated the sublevel spin population to understand the spin polarization of the isolated triplets.

To perform line shape analysis, we carried out the simulation of the EPR spectrum for an isolated triplet state under the consideration of the orientational motion caused by the triplet-exciton hopping between neighboring rubrene molecules in the presence of an external magnetic field.[69−71] Calculation procedures to obtain the simulated EPR spectrum are described in the Supporting Information. To obtain a simulated EPR spectrum, it is necessary to consider various

https://doi.org/10.1021/acs.jpclett.3c03602
J. Phys. Chem. Lett. 2024, 15, 2966−2975

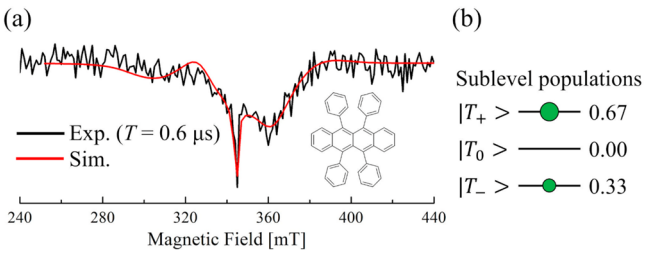

Figure 3. (a) Calculated spin-polarized EPR spectrum shown by the red line upon applying k_{hop} = 1 ns^{-1}. The TREPR spectrum observed at a 0.6 μs delay time is also shown (black). (b) Sublevel populations in the isolated triplet state used to obtain the red spectrum in (a). Population numbers are relative values among the triplet sublevels.

parameters. 1) The ZFS parameters, 2) the triplet sublevel populations, and 3) the hopping rate constant (k_{hop}) are the key parameters. The best combination of these parameters was obtained to reproduce the observed TREPR spectra. Figure 3a shows a simulated EPR spectrum using optimum parameters and the TREPR spectrum observed at a 0.6 μs delay time. The line shape of the simulated spectrum satisfactorily agrees with the experimental spectrum. First, ZFS parameters were determined to be D = 0.050 cm^{-1} with $|E|$ = 0.0052 cm^{-1}, where D and E represent magnetic anisotropies along the z axis and xy plane in the molecular-axis frame, respectively. In this experiment, several species of excitons are possible candidates for the origin of EPR signals. Parameterized ZFS thus helps us to identify the origin of the EPR signal. To our knowledge, ZFS parameters of rubrene have not been reported. However, D = 0.052 cm^{-1} and E = −0.0052 cm^{-1} in tetracene[66] are reasonably compatible with the present parameters of the ZFS for the rubrene which is the derivative of tetracene. Therefore, we confirmed that observed TREPR spectra originate from the triplet dynamics of rubrene undergoing TTA-UC.

Second, populations of isolated triplet-exciton sublevels were determined, as shown in Figure 3b. Populations in the upper sublevel $|T_+\rangle$ and the lower sublevel $|T_-\rangle$ are higher than that in $|T_0\rangle$, and the population of $|T_+\rangle$ is almost twice as large as that of $|T_-\rangle$. Third, the hopping rate constant k_{hop} was estimated. The simulated EPR spectra with various k_{hop} values in the rubrene system are shown in Figure S4. We found that an overall line shape of the simulated EPR spectrum with k_{hop} = 1 ns^{-1} is similar to that of the experimental spectrum. But the simulated spectrum does not reproduce a sharp emission signal observed at around 345 mT. This motional narrowing signal can be reproduced when $k_{hop} \geq$ 100 ns^{-1}. We note that we cannot estimate the order of the k_{hop} value accurately when k_{hop} is larger than 100 ns^{-1} because the susceptibility of the line shape to k_{hop} is small. As a result, the TREPR spectrum was

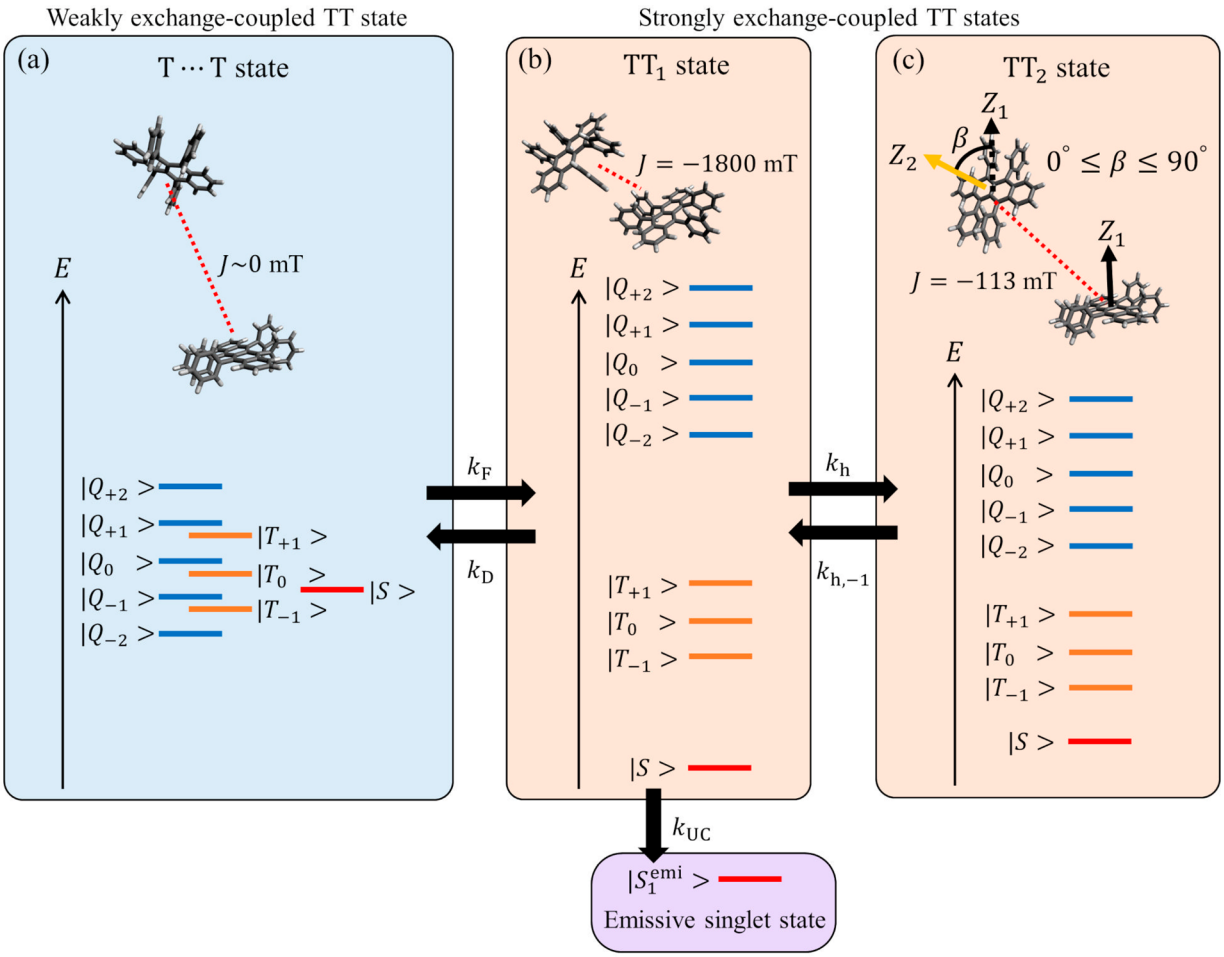

Figure 4. Spin states considered in our theoretical calculation model. k_F and k_D are the transition rate constants between (a) weakly exchange-coupled TT (T⋯T state) and (b, c) strongly exchange-coupled TTs (TT_1 and TT_2 states). In this study, we set these parameters as follows: k_F = 0.08 ns^{-1}, k_D = 1.0 ns^{-1}, k_h = 1.1 ns^{-1}, $k_{h,-1}$ = 1.0 ns^{-1}, and k_{UC} = 0.26 ns^{-1}. Parameters about the conformation of TTs are given in Table S3.

https://doi.org/10.1021/acs.jpclett.3c03602
J. Phys. Chem. Lett. 2024, 15, 2966−2975

completely reproduced by a summation of the two computed spectra of k_{hop} = 1 ns^{-1} and $k_{hop} \geq 100$ ns^{-1}. We thus found that most of triplets diffuse in the rubrene layer with k_{hop} = 1 ns^{-1} and that a small amount of those diffuse with $k_{hop} \geq 100$ ns^{-1}.

The k_{hop} value of the triplet exciton depends on the material morphology. In the following, we evaluate the validity of the above k_{hop} values. The k_{hop} can be obtained by using Smoluchowski−Einstein theory[72]

$$D_T = \frac{d^2}{6\tau_R} = \frac{k_{hop}d^2}{6} \quad (2)$$

where D_T is the translational diffusion constant, d is the distance between the chromophores, and τ_R is the hopping time between the chromophores that coincides with the reciprocal of k_{hop}. To calculate k_{hop}, d and D_T are required. In an amorphous solid, although the intermolecular distance of d is not known, we can assume that the averaged value of d is equal to the size of the unit cell of the single crystal because molecular packing is inhibited by the phenylene moieties in rubrene. We thus used d = 0.7 nm, which was the intermolecular distance along the b axis of a rubrene single crystal.[73] According to previous reports,[72,74,75] D_T for the triplet exciton in amorphous rubrene is 10^{-6}−10^{-7} cm^2 s^{-1} while D_T in the single crystal rubrene is 10^{-4}−10^{-5} cm^2 s^{-1}. By using these reported parameters, we estimate that k_{hop} is 0.12−1.2 ns^{-1} for amorphous rubrene and 12−120 ns^{-1} for single crystal rubrene, respectively. Compared with the k_{hop} values estimated by TREPR, k_{hop} = 1 ns^{-1} for most of the triplets is in the range of the amorphous region and $k_{hop} \geq 100$ ns^{-1} of those is in the range for the minor single crystal domain. This result is reasonable since the amorphous rubrene has been used in our TREPR measurements. Our result of the analysis implies that a small region of crystalline morphology is included in the rubrene film during our sample preparation process, although our process recipe has been developed to produce an amorphous rubrene film. It seems difficult to produce a perfect amorphous layer.

In this study, the EPR signal from the CT triplet state was not obtained. According to the result of a transient absorption measurement in a previous report,[59] the lifetime of the CT triplet in the rubrene/ITIC-Cl system is less than 1 ns, which is much shorter than the time resolution of our EPR apparatus (100 ns), so the CT triplet cannot be detected. One of the reasons for the quick triplet recombination dynamics is that the accumulated interfacial charges are created over a limited volume area in the present two-layer film (Figure 1a). In addition, the amorphous morphology in the rubrene layer plays a role in inducing the quick CT recombination because hole dissociation is inhibited from the interfacial CT state.

EPR signals of the quintet-TT states have often been observed in the SF system.[8,9,13,65,67,76] In the intermolecular SF systems of thin films, however, the triplet dissociation is entropically favorable compared with the strongly coupled TT at 80 K.[13] The absence of the quintet-TT states in the present system is consistent with the previous SF-induced triplet EPR in the TIPS-pentacene amorphous films[13] at 80 K and in the TIPS-tetracene thin films (>50 K), although quintet EPR was reported in the solute aggregates at 80 K.[65,67] In the linked SF systems, on the other hand, thermal activation is required to result in the weakened spin−spin exchange coupling in the triplet pairs by the dimer conformation changes, contributing to the strong quintet-TT signals. Unlike the SF system, because triplet diffusion is essential to generating the encountered TT state in the TTA system, it is highly challenging to detect the EPR signal of the quintet-TT state.

To understand the role of the dynamic conformation effect by $\mathbf{H}_{ZFS}$ on the spin conversion, we computed the sublevel spin population of the TT state during the TTA-UC process using a model based on our hypothesis in Scheme 1 for reproducing the spin polarization of the isolated triplet in Figure 3b. Figure 4 shows the simulation model considering a weakly exchange-coupled TT (blue part of Figure 4) and two types of strongly exchange-coupled TT states (orange parts of Figure 4). In the weak coupling (T···T), two triplets are not electronically coupled ($J \approx 0$ mT) due to the large distance between the excitons. When J is weaker than $\mathbf{H}_{ZFS}$, quintet−triplet−singlet mixings may occur through $\mathbf{H}_{ZFS}$.[9,13,76] The spin-state transition between the T···T state and the strongly exchange-coupled TT_1 state occurs with rate constants of k_F and k_D by the change in the distance between two diffusing triplets as shown in Figure 4. In the strongly exchange-coupled systems (Figure 4b,c), we define two types of states (a TT_1 state and a TT_2 state) with different mutual orientations between two triplets, i.e., molecular conformations of the TT states. In the amorphous rubrene film, the conformational change in the TT reasonably occurs by the intermolecular hopping of the triplet exciton between adjacent rubrene molecules. Such a conformational change also affects the J value because the exchange interaction originates from the overlaps of electron orbitals between the two triplets.[13] The conformational change is represented by the spin-state transition between the TT_1 (J = −1800 mT) and TT_2 (J = −113 mT) states with rate constants of k_h and $k_{h,-1}$. Due to the strong exchange interaction which is much larger than the Zeeman interaction ($g\mu_B B_0 \ll |J|$) for the TT_1 state, energy levels among $|S\rangle$, $|T_{m_{s,T}}\rangle$, and $|Q_{m_{s,Q}}\rangle$ sublevels are highly separated so that the spin interconversions among $|S\rangle$, $|T_{m_{s,T}}\rangle$, and $|Q_{m_{s,Q}}\rangle$ are inhibited. In the TT_2 state, the spin-state mixings are allowed by the level crossing mechanism[65] under an external magnetic field of about 340 mT, as mentioned in Scheme 1. The population in $|S\rangle$ in TT_1 is then transferred to the $|S_1^{semi}\rangle$ state with the rate constants of k_{UC}. The triplet TTA causing high-level reverse intersystem crossing is not considered at 80 K, because this is endothermic in rubrene.[52]

The spin Hamiltonians of the TT_1, TT_2, and T···T states are composed of the Zeeman interaction, ZFS interactions in the individual triplets, spin−spin dipolar coupling between the triplets, and exchange interaction between the triplets.[9] Energy levels of spin sublevels in the TT_1 state were calculated by diagonalization of the spin Hamiltonian. From the matrix elements of the magnitudes of the spin Hamiltonian calculated for the TT_2 state in the TT_1 basis, we confirmed that quintet−singlet mixings effectively occur and that the quintet−triplet and triplet−singlet mixings hardly occur (see Table S4). Therefore, the quintet−triplet and triplet−singlet spin interconversions in the strongly exchange-coupled states were ignored in this simulation. As an initial condition (T = 0 μs), we set the populations of the nine spin sublevels in the T···T state to be equally 11.1%. On the other hand, the populations in the TT_1 and TT_2 states were zero. Transition rates among three states (k_D, k_h, and $k_{h,-1}$) are set to be approximately 1 ns^{-1} from the hopping rate constant k_{hop} estimated in this study. The kinetics of the density matrix elements in the

https://doi.org/10.1021/acs.jpclett.3c03602
J. Phys. Chem. Lett. 2024, 15, 2966−2975

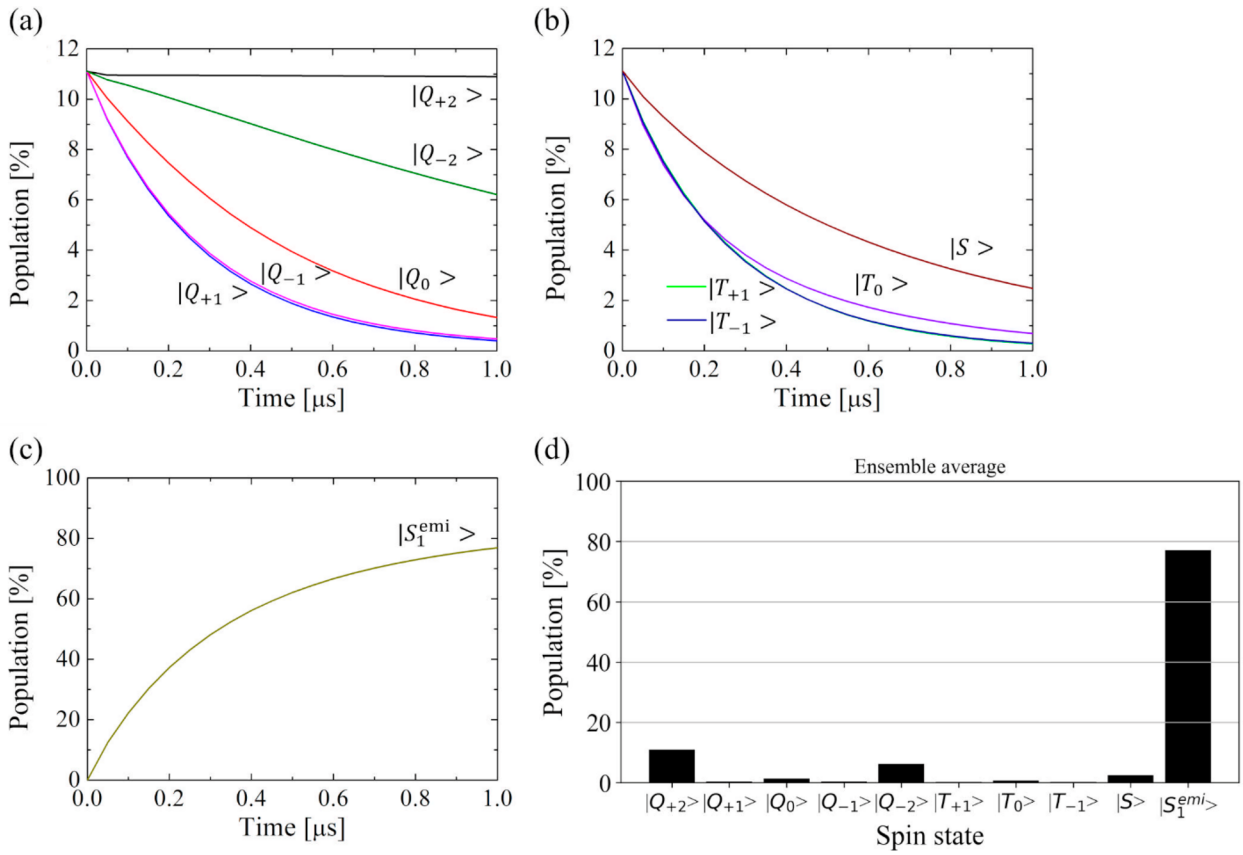

Figure 5. (a–c) Calculation results of spin population on the T···T state in the TT_1 basis for (a) five $|Q_{m_{s,Q}}\rangle$ sublevels, (b) three $|T_{m_{s,T}}\rangle$ sublevels and $|S\rangle$, and (c) an emissive singlet ($|S_1^{emi}\rangle$). (d) Summary of spin populations for all spin sublevels of the T···T state and $|S_1^{emi}\rangle$ state at T = 1.0 μs under an external magnetic field of 340 mT. The populations were calculated by taking an ensemble average over the various β values ($0° \leq \beta \leq 90°$).

diabatic TT_1 basis system was computed by solving coupled stochastic Liouville equations for the T···T, TT_1, and TT_2 states.[9,76] Because the matrices of the ZFS tensors in TT_1, TT_2, and T···T states are dependent on the orientations of the principal axes in the ZFS tensor ($\mathbf{D}_2$) for the second rubrene molecule with respect to the principal axes in the ZFS tensor ($\mathbf{D}_1$) for the first rubrene molecule, the principal axes in the $\mathbf{D}_2$ tensor are specified by using Euler rotation angles (α, β, and γ) with respect to the principal axes in the $\mathbf{D}_1$ tensor. In this computation (Figure 4), Euler rotation angles were set to be representative values in the TT_1 and T···T states. Alternatively, as shown in Figure 4c, various angles (β) in TT_2 states are considered because we expect that the sublevel spin populations are represented by an ensemble average from the various TT_2 conformations in the amorphous solid. This is relevant to the random orientation dynamics concluded from the line-shape analysis of the TREPR spectra. The details and parameters of the computing method are described in the Supporting Information, section 6. Simulation results of the populations of all spin sublevels in the T···T state and the S_1^{emi} state from T = 0.0 to 1.0 μs under an external magnetic field of 340 mT are shown in Figure 5. The population of the S_1^{emi} state gradually increases and reached 77.0% at T = 1.0 μs. On the other hand, the populations of all nine spin sublevels in the T··· T state gradually decrease. Differences in depopulation rates among sublevels reflect the anisotropy of the ZFS interaction, strength of the exchange interaction, and spin-state transition rate constants. We summarize the populations of all spin sublevels in the T···T state and the S_1^{emi} state at T = 0.0 and 1.0 μs in Table S8. Remarkably, at T = 1.0 μs, the resultant populations of $|Q_{+2}\rangle$ and $|Q_{-2}\rangle$ sublevels are 10.9 and 6.2%, which are larger than those of other sublevels. Resultant excitons are finally dissociated to isolated triplets, which maintain the ESP derived through the TTA process. As shown in the yellow part of Scheme 1, in the high-field approximation, spin wave functions of $|Q_{+2}\rangle$ and $|Q_{-2}\rangle$ sublevels are represented by using the spin wave functions of individual triplet sublevels T_+ and T_- as follows: $|Q_{+2}\rangle = |T_+\ T_+\rangle$ and $|Q_{-2}\rangle = |T_-\ T_-\rangle$, respectively.[77] Thus, the populations in $|Q_{+2}\rangle$ and $|Q_{-2}\rangle$ sublevels in the T···T state result in $|T_+\rangle$ and $|T_-\rangle$ sublevel populations in the individual triplet states, respectively. This is coincident with the ESP estimated by our TREPR measurements, as shown in Figure 3b. Thus, we confirmed that the present conformation model causing the spin-state mixing reasonably explains the emissive and asymmetric TREPR pattern in Figure 3.

The dependences of angle β in the TT_2 state on the sublevel spin populations in the T···T state under the external magnetic field of 340 mT are shown in Figure S6. We found that the populations in the T···T state depend on β while its dependence is small. This indicates that the TTA-UC proceeds without much restriction on the molecular conformation in the amorphous rubrene system. Furthermore, we also calculated the population of the S_1^{emi} state at zero field (0 mT). It is notable that the population of the S_1^{emi} state, corresponding to η in this computation, reaches 77.5% at T = 1.0 μs (Figures S7

https://doi.org/10.1021/acs.jpclett.3c03602
J. Phys. Chem. Lett. 2024, 15, 2966−2975

and S8), which agrees with a previous report of η = 64% on the amorphous rubrene system.[57,58] The high η is thus due to the following. First, from the matrix elements of the spin Hamiltonian calculated for the TT_2 state and the T···T state at zero field (Tables S6 and S7), it is clear that the quintet-to-singlet spin interconversions in the TT_2 state and the triplet-to-quintet and quintet-to-singlet spin interconversions in the T···T state occur efficiently. Second, the intermolecular hopping rate of the triplet exciton (k_{hop} = 1 ns^{-1}) plays an effective role in increasing the population of the $|S\rangle$ state. The slower the exciton diffusion, the more efficient the spin state mixing by the ZFS-induced level-crossing mechanism. Previously, a similar mechanism was demonstrated in the chemically induced dynamic electron polarization (CIDEP) systems with radical-triplet pairs for $D_T < 10^{-5}$ cm^2 s^{-1}.[78] Since D_T of an amorphous rubrene film (10^{-6}–10^{-7} cm^2 s^{-1}) exhibits values smaller than 10^{-5} cm^2 s^{-1}, the spin state mixings will take place effectively.[65] In addition, random exciton hopping induces modulations of exchange interactions originating from the modulation of the distance or of the molecular orientation between two triplets. Thanks to the molecular conformation dynamics by random exciton hopping with k_{hop} = 1 ns^{-1}, the spin sublevels of the TT state are mixed at the level-crossing region efficiently during the TTA process. The above mixing mechanism thus contributes to the efficient spin population transfers from $|T_{m_{s,T}}\rangle$ and $|Q_{m_{s,Q}}\rangle$ to $|S\rangle$ in the TT and to the realization of high η in the amorphous rubrene layer, causing the emissive spin polarization in the residual triplets.

In conclusion, we investigated the spin dynamics in the TTA process in a rubrene/ITIC-Cl bilayer film, which was known as a highly efficient TTA-UC system in the solid state. We observed the spin-polarized separated triplet state in the rubrene layer by the TREPR method and estimated the intermolecular hopping rate of the triplet exciton. We proposed a theoretical model about the spin dynamics on the TTA process to interpret the TREPR results and simulated the ESP of the exchange-coupled TT state by utilizing several parameters such as the ZFS constant and the hopping rate constant determined by TREPR. Simulation result shows that the efficient triplet-to-quintet and quintet-to-singlet spin interconversions induced by anisotropic ZFS interaction occur during the TTA process, and the modulation of exchange interaction in the TT state with a rate constant of 1 ns^{-1} reinforces the spin population transfer from $|T_{m_{s,T}}\rangle$ and $|Q_{m_{s,Q}}\rangle$ sublevels to $|S\rangle$. We also note that the exciton diffusion with random orientation dynamics between the two triplets causes the modulation of the exchange interaction. We concluded that such molecular conformation dynamics contributes to the improvement of η in the amorphous rubrene film. Our findings for the spin interconversion mechanism in the TTA-UC system may act as a guide to the development of novel materials exhibiting highly efficient light-to-energy conversion systems.[79]

■ ASSOCIATED CONTENT

Supporting Information

The Supporting Information is available free of charge at https://pubs.acs.org/doi/10.1021/acs.jpclett.3c03602.

Temperature dependence of TTA-UC emission intensity, dependence of the excitation light power density on the intensity of the EPR signal, calculation procedure to obtain the simulated EPR spectra, computational method to obtain the ESP in the TT states, and the results of these simulations (PDF)

Transparent Peer Review report available (PDF)

■ AUTHOR INFORMATION

Corresponding Authors

Tsubasa Okamoto − *Molecular Photoscience Research Center, Kobe University, Kobe 657-8501, Japan; Department of Chemistry, Graduate School of Science, Kobe University, Kobe 657−8501, Japan;* orcid.org/0000-0003-4178-4588; Email: t-okamoto@phoenix.kobe-u.ac.jp

Seiichiro Izawa − *Laboratory for Materials and Structures, Institute of Innovative Research, Tokyo Institute of Technology, Yokohama, Kanagawa 226-8503, Japan; Institute for Molecular Science, Okazaki, Aichi 444-8787, Japan; Precursory Research for Embryonic Science and Technology (PRESTO), Japan Science and Technology Agency (JST), Kawaguchi, Saitama 332-0012, Japan;* orcid.org/0000-0002-1761-2682; Email: izawa.s.ac@m.titech.ac.jp

Yasuhiro Kobori − *Molecular Photoscience Research Center, Kobe University, Kobe 657-8501, Japan; Department of Chemistry, Graduate School of Science, Kobe University, Kobe 657−8501, Japan; CREST, JST, Kawaguchi, Saitama 332-0012, Japan;* orcid.org/0000-0001-8370-9362; Email: ykobori@kitty.kobe-u.ac.jp

Author

Masahiro Hiramoto − *Institute for Molecular Science, Okazaki, Aichi 444-8787, Japan;* orcid.org/0000-0002-7190-7633

Complete contact information is available at: https://pubs.acs.org/10.1021/acs.jpclett.3c03602

Notes

The authors declare no competing financial interest.

■ ACKNOWLEDGMENTS

This work was partially supported by a JSPS KAKENHI Grant-in-Aid for Transformative Research Areas "Dynamic Exciton" (JP20H05832 to Y.K. and JP21H05411 to S.I.), grant nos. JP22K19008 and JP20K21174 to Y.K and JP22K14648 to T.O., JST PRESTO (JPMJPR2101) to S.I., and a Yukawa Memorial Foundation grant to T.O.

■ REFERENCES

(1) Merrifield, R. E. Magnetic effects on triplet exciton interactions. *Pure Appl. Chem.* **1971**, *27* (3), 481−498.

(2) Yong, C. K.; Musser, A. J.; Bayliss, S. L.; Lukman, S.; Tamura, H.; Bubnova, O.; Hallani, R. K.; Meneau, A.; Resel, R.; Maruyama, M.; et al. The entangled triplet pair state in acene and heteroacene materials. *Nat. Commun.* **2017**, *8*, 15953.

(3) Avakian, P. Influence of magnetic fields on luminescence involving triplet excitons. *Pure Appl. Chem.* **1974**, *37* (1−2), 1−19.

(4) Groff, R. P.; Avakian, P.; Merrifield, R. E. Coexistence of Exciton Fission and Fusion in Tetracene Crystals. *Phys. Rev. B* **1970**, *1* (2), 815−817.

(5) Merrifield, R. E. Theory of Magnetic Field Effects on the Mutual Annihilation of Triplet Excitons. *J. Chem. Phys.* **1968**, *48* (9), 4318−4319.

(6) Johnson, R. C.; Merrifield, R. E.; Avakian, P.; Flippen, R. B. Effects of Magnetic Fields on the Mutual Annihilation of Triplet Excitons in Molecular Crystals. *Phys. Rev. Lett.* **1967**, *19* (6), 285−287.

(7) Kepler, R. G.; Caris, J. C.; Avakian, P.; Abramson, E. Triplet excitons and Delayed Fluorescence in Anthracene Crystals. *Phys. Rev. Lett.* **1963**, *10* (9), 400−402.
(8) Tayebjee, M. J. Y.; Sanders, S. N.; Kumarasamy, E.; Campos, L. M.; Sfeir, M. Y.; McCamey, D. R. Quintet multiexciton dynamics in singlet fission. *Nat. Phys.* **2017**, *13* (2), 182−188.
(9) Kobori, Y.; Fuki, M.; Nakamura, S.; Hasobe, T. Geometries and Terahertz Motions Driving Quintet Multiexcitons and Ultimate Triplet-Triplet Dissociations via the Intramolecular Singlet Fissions. *J. Phys. Chem. B* **2020**, *124* (42), 9411−9419.
(10) Yago, T.; Tashiro, M.; Hasegawa, K.; Gohdo, M.; Tsuchiya, S.; Ikoma, T.; Wakasa, M. Triplet-Triplet Annihilation via the Triplet Channel in Crystalline 9,10-Diphenylanthracene. *J. Phys. Chem. Lett.* **2022**, *13* (37), 8768−8774.
(11) Bardeen, C. J. Time dependent correlations of entangled states with nondegenerate branches and possible experimental realization using singlet fission. *J. Chem. Phys.* **2019**, *151* (12), No. 124503.
(12) Scholes, G. D. Correlated Pair States Formed by Singlet Fission and Exciton-Exciton Annihilation. *J. Phys. Chem. A* **2015**, *119* (51), 12699−12705.
(13) Matsuda, S.; Oyama, S.; Kobori, Y. Electron spin polarization generated by transport of singlet and quintet multiexcitons to spin-correlated triplet pairs during singlet fissions. *Chem. Sci.* **2020**, *11* (11), 2934−2942.
(14) Musser, A. J.; Clark, J. Triplet-Pair States in Organic Semiconductors. *Annu. Rev. Phys. Chem.* **2019**, *70*, 323−351.
(15) Smyser, K. E.; Eaves, J. D. Singlet fission for quantum information and quantum computing: the parallel JDE model. *Sci. Rep* **2020**, *10* (1), No. 18480.
(16) Jacobberger, R. M.; Qiu, Y.; Williams, M. L.; Krzyaniak, M. D.; Wasielewski, M. R. Using Molecular Design to Enhance the Coherence Time of Quintet Multiexcitons Generated by Singlet Fission in Single Crystals. *J. Am. Chem. Soc.* **2022**, *144* (5), 2276−2283.
(17) Yang, Z. Y.; Mao, Z.; Xie, Z. L.; Zhang, Y.; Liu, S. W.; Zhao, J.; Xu, J. R.; Chi, Z. G.; Aldred, M. P. Recent advances in organic thermally activated delayed fluorescence materials. *Chem. Soc. Rev.* **2017**, *46* (3), 915−1016.
(18) Kondakov, D. Y. Triplet-triplet annihilation in highly efficient fluorescent organic light-emitting diodes: current state and future outlook. *Philos. Trans A Math Phys. Eng. Sci.* **2015**, *373* (2044), No. 20140321.
(19) Suzuki, T.; Nonaka, Y.; Watabe, T.; Nakashima, H.; Seo, S.; Shitagaki, S.; Yamazaki, S. Highly efficient long-life blue fluorescent organic light-emitting diode exhibiting triplet−triplet annihilation effects enhanced by a novel hole-transporting material. *Jpn. J. Appl. Phys.* **2014**, *53* (5), No. 052102.
(20) Kondakov, D. Y.; Pawlik, T. D.; Hatwar, T. K.; Spindler, J. P. Triplet annihilation exceeding spin statistical limit in highly efficient fluorescent organic light-emitting diodes. *J. Appl. Phys.* **2009**, *106* (12), No. 124510.
(21) Izawa, S.; Morimoto, M.; Naka, S.; Hiramoto, M. Efficient Interfacial Upconversion Enabling Bright Emission at an Extremely Low Driving Voltage in Organic Light-Emitting Diodes. *Adv. Opt Mater.* **2022**, *10* (4), No. 2101710.
(22) Izawa, S.; Morimoto, M.; Fujimoto, K.; Banno, K.; Majima, Y.; Takahashi, M.; Naka, S.; Hiramoto, M. Blue organic light-emitting diode with a turn-on voltage of 1.47 V. *Nat. Commun.* **2023**, *14* (1), 5494.
(23) Dilbeck, T.; Hanson, K. Molecular Photon Upconversion Solar Cells Using Multilayer Assemblies: Progress and Prospects. *J. Phys. Chem. Lett.* **2018**, *9* (19), 5810−5821.
(24) Frazer, L.; Gallaher, J. K.; Schmidt, T. W. Optimizing the Efficiency of Solar Photon Upconversion. *ACS Energy Lett.* **2017**, *2* (6), 1346−1354.
(25) Goldschmidt, J. C.; Fischer, S. Upconversion for Photovoltaics - a Review of Materials, Devices and Concepts for Performance Enhancement. *Adv. Opt Mater.* **2015**, *3* (4), 510−535.
(26) Gray, V.; Dzebo, D.; Abrahamsson, M.; Albinsson, B.; Moth-Poulsen, K. Triplet-triplet annihilation photon-upconversion: towards solar energy applications. *Phys. Chem. Chem. Phys.* **2014**, *16* (22), 10345−10352.
(27) Nattestad, A.; Cheng, Y. Y.; MacQueen, R. W.; Schulze, T. F.; Thompson, F. W.; Mozer, A. J.; Fuckel, B.; Khoury, T.; Crossley, M. J.; Lips, K.; et al. Dye-Sensitized Solar Cell with Integrated Triplet-Triplet Annihilation Upconversion System. *J. Phys. Chem. Lett.* **2013**, *4* (12), 2073−2078.
(28) Tayebjee, M. J.; McCamey, D. R.; Schmidt, T. W. Beyond Shockley-Queisser: Molecular Approaches to High-Efficiency Photovoltaics. *J. Phys. Chem. Lett.* **2015**, *6* (12), 2367−2378.
(29) Hill, S. P.; Hanson, K. Harnessing Molecular Photon Upconversion in a Solar Cell at Sub-solar Irradiance: Role of the Redox Mediator. *J. Am. Chem. Soc.* **2017**, *139* (32), 10988−10991.
(30) Wu, S.; Butt, H. J. Near-Infrared-Sensitive Materials Based on Upconverting Nanoparticles. *Adv. Mater.* **2016**, *28* (6), 1208−1226.
(31) Zhou, J.; Liu, Q.; Feng, W.; Sun, Y.; Li, F. Y. Upconversion Luminescent Materials: Advances and Applications. *Chem. Rev.* **2015**, *115* (1), 395−465.
(32) Tu, L.; Liu, X.; Wu, F.; Zhang, H. Excitation energy migration dynamics in upconversion nanomaterials. *Chem. Soc. Rev.* **2015**, *44* (6), 1331−1345.
(33) Huang, L.; Kakadiaris, E.; Vaneckova, T.; Huang, K.; Vaculovicova, M.; Han, G. Designing next generation of photon upconversion: Recent advances in organic triplet-triplet annihilation upconversion nanoparticles. *Biomaterials* **2019**, *201*, 77−86.
(34) Liu, Y.; Meng, X.; Bu, W. Upconversion-based photodynamic cancer therapy. *Coordin Chem. Rev.* **2019**, *379*, 82−98.
(35) Wang, W. P.; Liu, Q.; Zhan, C. Y.; Barhoumi, A.; Yang, T. S.; Wylie, R. G.; Armstrong, P. A.; Kohane, D. S. Efficient Triplet-Triplet Annihilation-Based Upconversion for Nanoparticle Phototargeting. *Nano Lett.* **2015**, *15* (10), 6332−6338.
(36) Sasaki, Y.; Oshikawa, M.; Bharmoria, P.; Kouno, H.; Hayashi-Takagi, A.; Sato, M.; Ajioka, I.; Yanai, N.; Kimizuka, N. Near-Infrared Optogenetic Genome Engineering Based on Photon-Upconversion Hydrogels. *Angew. Chem. Int. Edit* **2019**, *58* (49), 17827−17833.
(37) Wan, Y.; Guo, Z.; Zhu, T.; Yan, S. X.; Johnson, J.; Huang, L. B. Cooperative singlet and triplet exciton transport in tetracene crystals visualized by ultrafast microscopy. *Nat. Chem.* **2015**, *7* (10), 785−792.
(38) Schmidt, T. W.; Castellano, F. N. Photochemical Upconversion: The Primacy of Kinetics. *J. Phys. Chem. Lett.* **2014**, *5* (22), 4062−4072.
(39) Gray, V.; Dreos, A.; Erhart, P.; Albinsson, B.; Moth-Poulsen, K.; Abrahamsson, M. Loss channels in triplet-triplet annihilation photon upconversion: importance of annihilator singlet and triplet surface shapes. *Phys. Chem. Chem. Phys.* **2017**, *19* (17), 10931−10939.
(40) Olesund, A.; Gray, V.; Martensson, J.; Albinsson, B. Diphenylanthracene Dimers for Triplet-Triplet Annihilation Photon Upconversion: Mechanistic Insights for Intramolecular Pathways and the Importance of Molecular Geometry. *J. Am. Chem. Soc.* **2021**, *143* (15), 5745−5754.
(41) Johnson, R. C.; Merrifield, R. E. Effects of Magnetic Fields on the Mutual Annihilation of Triplet Excitons in Anthracene Crystals. *Phys. Rev. B* **1970**, *1* (2), 896−902.
(42) Bharmoria, P.; Bildirir, H.; Moth-Poulsen, K. Triplet-triplet annihilation based near infrared to visible molecular photon upconversion. *Chem. Soc. Rev.* **2020**, *49* (18), 6529−6554.
(43) Hoseinkhani, S.; Tubino, R.; Meinardi, F.; Monguzzi, A. Achieving the photon up-conversion thermodynamic yield upper limit by sensitized triplet-triplet annihilation. *Phys. Chem. Chem. Phys.* **2015**, *17* (6), 4020−4024.
(44) Schulze, T. F.; Schmidt, T. W. Photochemical upconversion: present status and prospects for its application to solar energy conversion. *Energ Environ. Sci.* **2015**, *8* (1), 103−125.
(45) Singh-Rachford, T. N.; Castellano, F. N. Photon upconversion based on sensitized triplet-triplet annihilation. *Coordin Chem. Rev.* **2010**, *254* (21−22), 2560−2573.

https://doi.org/10.1021/acs.jpclett.3c03602
J. Phys. Chem. Lett. 2024, 15, 2966−2975

(46) Wong, M. Y.; Zysman-Colman, E. Purely Organic Thermally Activated Delayed Fluorescence Materials for Organic Light-Emitting Diodes. *Adv. Mater.* **2017**, *29* (22), 1605444.
(47) Cheng, Y. Y.; Fuckel, B.; Khoury, T.; Clady, R. G. C. R.; Tayebjee, M. J. Y.; Ekins-Daukes, N. J.; Crossley, M. J.; Schmidt, T. W. Kinetic Analysis of Photochemical Upconversion by Triplet-Triplet Annihilation: Beyond Any Spin Statistical Limit. *J. Phys. Chem. Lett.* **2010**, *1* (12), 1795−1799.
(48) Sun, W. J.; Ronchi, A.; Zhao, T. H.; Han, J. L.; Monguzzi, A.; Duan, P. F. Highly efficient photon upconversion based on triplet-triplet annihilation from bichromophoric annihilators. *Journal of Materials Chemistry C* **2021**, *9* (40), 14201−14208.
(49) Harada, N.; Sasaki, Y.; Hosoyamada, M.; Kimizuka, N.; Yanai, N. Discovery of Key TIPS-Naphthalene for Efficient Visible-to-UV Photon Upconversion under Sunlight and Room Light*. *Angew. Chem., Int. Ed. Engl.* **2021**, *60* (1), 142−147.
(50) Hou, L.; Olesund, A.; Thurakkal, S.; Zhang, X.; Albinsson, B. Efficient Visible-to-UV Photon Upconversion Systems Based on CdS Nanocrystals Modified with Triplet Energy Mediators. *Adv. Funct. Mater.* **2021**, *31* (47), No. 2106198.
(51) Olesund, A.; Johnsson, J.; Edhborg, F.; Ghasemi, S.; Moth-Poulsen, K.; Albinsson, B. Approaching the Spin-Statistical Limit in Visible-to-Ultraviolet Photon Upconversion. *J. Am. Chem. Soc.* **2022**, *144* (8), 3706−3716.
(52) Bossanyi, D. G.; Sasaki, Y.; Wang, S.; Chekulaev, D.; Kimizuka, N.; Yanai, N.; Clark, J. Spin Statistics for Triplet-Triplet Annihilation Upconversion: Exchange Coupling, Intermolecular Orientation, and Reverse Intersystem Crossing. *JACS Au* **2021**, *1* (12), 2188−2201.
(53) Ha, D. G.; Wan, R.; Kim, C. A.; Lin, T. A.; Yang, L.; Van Voorhis, T.; Baldo, M. A.; Dinca, M. Exchange controlled triplet fusion in metal-organic frameworks. *Nat. Mater.* **2022**, *21* (11), 1275−1281.
(54) Atkins, P. W.; Evans, G. T. Magnetic field effects on chemiluminescent fluid solutions. *Mol. Phys.* **1975**, *29* (3), 921−935.
(55) Yokoyama, K.; Wakikawa, Y.; Miura, T.; Fujimori, J.; Ito, F.; Ikoma, T. Solvent Viscosity Effect on Triplet-Triplet Pair in Triplet Fusion. *J. Phys. Chem. B* **2015**, *119* (52), 15901−15908.
(56) Mani, T.; Vinogradov, S. A. Magnetic Field Effects on Triplet-Triplet Annihilation in Solutions: Modulation of Visible/NIR Luminescence. *J. Phys. Chem. Lett.* **2013**, *4* (17), 2799−2804.
(57) Izawa, S.; Hiramoto, M. Efficient solid-state photon upconversion enabled by triplet formation at an organic semiconductor interface. *Nat. Photonics* **2021**, *15* (12), 895−900.
(58) Di, D.; Yang, L.; Richter, J. M.; Meraldi, L.; Altamimi, R. M.; Alyamani, A. Y.; Credgington, D.; Musselman, K. P.; MacManus-Driscoll, J. L.; Friend, R. H. Efficient Triplet Exciton Fusion in Molecularly Doped Polymer Light-Emitting Diodes. *Adv. Mater.* **2017**, *29* (13), No. 1605987.
(59) Sakamoto, Y.; Izawa, S.; Ohkita, H.; Hiramoto, M.; Tamai, Y. Triplet sensitization via charge recombination at organic heterojunction for efficient near-infrared to visible solid-state photon upconversion. *Communications Materials* **2022**, *3* (1), 76.
(60) Firdaus, Y.; Le Corre, V. M.; Karuthedath, S.; Liu, W. L.; Markina, A.; Huang, W. T.; Chattopadhyay, S.; Nahid, M. M.; Nugraha, M. I.; Lin, Y. B.; et al. Long-range exciton diffusion in molecular non-fullerene acceptors. *Nat. Commun.* **2020**, *11* (1), 5220.
(61) Sajjad, M. T.; Ruseckas, A.; Jagadamma, L. K.; Zhang, Y. W.; Samuel, I. D. W. Long-range exciton diffusion in non-fullerene acceptors and coarse bulk heterojunctions enable highly efficient organic photovoltaics. *J. Mater. Chem. A* **2020**, *8* (31), 15687−15694.
(62) Natsuda, S.; Sakamoto, Y.; Takeyama, T.; Shirouchi, R.; Saito, T.; Tamai, Y.; Ohkita, H. Singlet and Triplet Excited-State Dynamics of a Nonfullerene Electron Acceptor Y6. *J. Phys. Chem. C* **2021**, *125* (38), 20806−20813.
(63) Chandrabose, S.; Chen, K.; Barker, A. J.; Sutton, J. J.; Prasad, S. K. K.; Zhu, J. S.; Zhou, J. D.; Gordon, K. C.; Xie, Z. Q.; Zhan, X. W.; et al. High Exciton Diffusion Coefficients in Fused Ring Electron Acceptor Films. *J. Am. Chem. Soc.* **2019**, *141* (17), 6922−6929.
(64) Haefele, A.; Blumhoff, J.; Khnayzer, R. S.; Castellano, F. N. Getting to the (Square) Root of the Problem: How to Make Noncoherent Pumped Upconversion Linear. *J. Phys. Chem. Lett.* **2012**, *3* (3), 299−303.
(65) Nagashima, H.; Kawaoka, S.; Akimoto, S.; Tachikawa, T.; Matsui, Y.; Ikeda, H.; Kobori, Y. Singlet-Fission-Born Quintet State: Sublevel Selections and Trapping by Multiexciton Thermodynamics. *J. Phys. Chem. Lett.* **2018**, *9* (19), 5855−5861.
(66) Yarmus, L.; Rosentha, J.; Chopp, M. Epr of Triplet Excitons in Tetracene Crystals - Spin Polarization and Role of Singlet Exciton Fission. *Chem. Phys. Lett.* **1972**, *16* (3), 477−481.
(67) Weiss, L. R.; Bayliss, S. L.; Kraffert, F.; Thorley, K. J.; Anthony, J. E.; Bittl, R.; Friend, R. H.; Rao, A.; Greenham, N. C.; Behrends, J. Strongly exchange-coupled triplet pairs in an organic semiconductor. *Nat. Phys.* **2017**, *13* (2), 176−181.
(68) Sillescu, H. Theory of Molecular Reorientation in Liquids: Magnetic Spin Resonance Line Shapes. *J. Chem. Phys.* **1971**, *54* (5), 2110−2119.
(69) Kitagawa, H.; Kobori, Y.; Yamanaka, M.; Yoza, K.; Kobayashi, K. Molecular recognition and self-assembly special feature: Encapsulated-guest rotation in a self-assembled heterocapsule directed toward a supramolecular gyroscope. *Proc. Natl. Acad. Sci. U. S. A.* **2009**, *106* (26), 10444−10448.
(70) Yamauchi, S.; Takahashi, A.; Iwasaki, Y.; Unno, M.; Ohba, Y.; Higuchi, J.; Blank, A.; Levanon, H. The Lowest Photoexcited Triplet State of Subphthalocyanine in Solid and Fluid Environments. Time-Resolved Electron Paramagnetic Resonance Studies. *J. Phys. Chem. A* **2003**, *107* (10), 1478−1485.
(71) Han, Y.; Hamada, M.; Chang, I. Y.; Hyeon-Deuk, K.; Kobori, Y.; Kobayashi, Y. Fast T-Type Photochromism of Colloidal Cu-Doped ZnS Nanocrystals. *J. Am. Chem. Soc.* **2021**, *143* (5), 2239−2249.
(72) Mikhnenko, O. V.; Blom, P. W. M.; Nguyen, T. Q. Exciton diffusion in organic semiconductors. *Energ Environ. Sci.* **2015**, *8* (7), 1867−1888.
(73) Nitta, J.; Miwa, K.; Komiya, N.; Annese, E.; Fujii, J.; Ono, S.; Sakamotat, K. The actual electronic band structure of a rubrene single crystal. *Sci. Rep-Uk* **2019**, *9*, 9645.
(74) Radiunas, E.; Dapkevičius, M.; Raišys, S.; Kazlauskas, K. Triplet and singlet exciton diffusion in disordered rubrene films: implications for photon upconversion. *Phys. Chem. Chem. Phys.* **2022**, *24* (39), 24345−24352.
(75) Irkhin, P.; Biaggio, I.; Zimmerling, T.; Döbeli, M.; Batlogg, B. Defect density dependent photoluminescence yield and triplet diffusion length in rubrene. *Appl. Phys. Lett.* **2016**, *108* (6), No. 063302.
(76) Nakamura, S.; Sakai, H.; Nagashima, H.; Fuki, M.; Onishi, K.; Khan, R.; Kobori, Y.; Tkachenko, N. V.; Hasobe, T. Synergetic Role of Conformational Flexibility and Electronic Coupling for Quantitative Intramolecular Singlet Fission. *J. Phys. Chem. C* **2021**, *125* (33), 18287−18296.
(77) Benk, H.; Sixl, H. Theory of two coupled triplet states. *Mol. Phys.* **1981**, *42* (4), 779−801.
(78) Kobori, Y.; Takeda, K.; Tsuji, K.; Kawai, A.; Obi, K. Exchange Interaction in Radical−Triplet Pairs: Evidences for CIDEP Generation by Level Crossings in Triplet−Doublet Interactions. *J. Phys. Chem. A* **1998**, *102* (27), 5160−5170.
(79) Imahori, H.; Kobori, Y.; Kaji, H. Manipulation of Charge-Transfer States by Molecular Design: Perspective from "Dynamic Exciton". *Acc. Mater. Res.* **2021**, *2* (7), 501−514.

https://doi.org/10.1021/acs.jpclett.3c03602
J. Phys. Chem. Lett. 2024, 15, 2966−2975